ACS OMEGA

Open Access

http://pubs.acs.org/journal/acsodf

Article

Transparent and High-Refractive-Index Titanium Dioxide/Thermoplastic Polyurethane Nanocomposites

Massimo Tawfilas, Gianluca Bartolini Torres, Roberto Lorenzi, Melissa Saibene, Michele Mauri, and Roberto Simonutti*

Cite This: *ACS Omega* 2024, 9, 29339−29349

Read Online

ACCESS | Metrics & More | Article Recommendations | Supporting Information

ABSTRACT: Transparent nanocomposite films made of surface-modified titanium dioxide nanoparticles and thermoplastic polyurethane are prepared via film casting approach showing enhanced refractive indexes and mechanical properties. Two different sets of composites were prepared up to 37.5 wt % of inorganic nanoparticles with a diameter <15 nm, one set using particles capped only with oleic acid and a second one with a bimodal system layer made of oleic acid and mPEO-5000 as coating agents. All of the composites show significantly enhanced refractive index and mechanical properties than the neat polymeric matrix. The transparency of nanocomposite films shows the excellent dispersion of the inorganic nanoparticles in the polymeric matrix avoiding aggregation and precipitation phenomena. Our study provides a facile and feasible route to produce transparent nanocomposite films with tunable mechanical properties and high refractive indices for various applications.

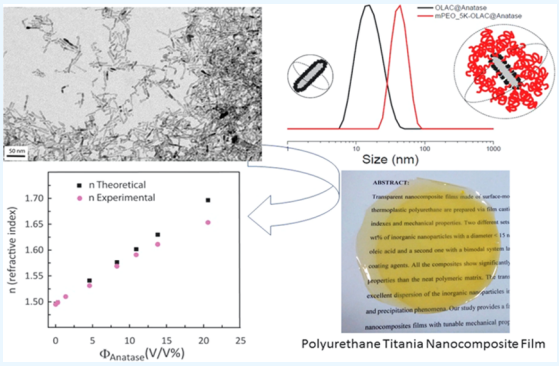

1. INTRODUCTION

Polymeric materials display a large variety of mechanical properties as a function of chemical structure and processing procedures. Thermoplastic elastomers combine the ease of transformation typical of thermoplastic polymers with the properties of elastomers, and for this reason, they find an increasing range of applications.[1] Among others, thermoplastic polyurethanes (TPU) are very interesting, since their composition involves several comonomers and thus allows several avenues of modulating their mechanical and viscoelastic properties.[2] As an example, by varying the length of the polyol, it is possible to increase or decrease the glass transition temperature.[3]

In some cases, TPUs are transparent in the visible spectrum region, but their low refractive index limits their use in advanced optical applications such as microlenses, image sensors, and organic light-emitting diodes. A possible approach to improve their optical properties is to act on the chemistry of the polymer chains. The insertion of heavy atoms in the backbone of the polymer or in the side branching can be quite efficient in increasing the refractive index.[4] In the recent years, research has especially focused on the incorporation of sulfur atoms.[5,6] However, in the case of industrial polymers, such as TPUs, that are manufactured on a large scale with well-established processes, alternative approaches should be pursued, especially in the production of consumer goods.

An interesting suitable solution is the introduction of inorganic nanoparticles (NPs) endowed with high refractive index into polymer matrixes.[7] These systems, defined as polymer nanocomposites,[8] according to Rayleigh's law are transparent when the dispersed phase is smaller than 40 nm.[9] A family of nanocomposites widely reported in the literature is based on titanium dioxide NPs, since TiO_2 has a relatively large refractive index (n = 2.45 and 2.7 at 500 nm for anatase and rutile phases, respectively),[10] has no absorptions in the visible light range, and can be easily produced as nanocrystals with controlled size and shape.[11]

However, most inorganic nanoparticles present high surface energies and do not aggregate only in the presence of polymers bearing functional groups able to interact with the surface,[12,13] but when the polymer matrix is almost apolar, as in the case of PU, aggregation is unavoidable. Large aggregates determine high scattering intensity of visible light causing a turbid appearance of the nanocomposite,[14] limiting optical applications.

A strategy for minimizing interface energy is the modification of the surface of the nanoparticles by using small molecules[15] or by polymer grafting, producing the so-called polymer-grafted nanoparticles or PGNs.[16] This method

Received: February 1, 2024
Revised: May 2, 2024
Accepted: May 27, 2024
Published: June 24, 2024

creates a thin polymer layer on the nanoparticles that reduces the particle−particle interaction and favors the dispersion of the particles in the polymer bulk. The two main synthetic routes followed are the grafting-to and grafting-from approach.[17] In the grafting-to method, a preformed and end-functionalized polymer is attached to the surface. The inorganic surface reactivity to end-functionalized polymers and their interaction with the solvent in which the reaction takes place drive the grafting-to process. The grafting-to method is easily implemented but presents several drawbacks. Steric repulsion from the polymer chains already attached hampers chain diffusion to the surface, thus limiting the available graft density. In general, the obtained PGNc are sparsely covered, and the sections of polymer farthest from the surface tend to conform in a random coil: the result is the so-called mushroom-like conformation.[18] The grafting-from method is a surface-initiated polymerization started with an initiator or chain transfer agent.[19] The diffusion of a relatively small monomer to the surface[20] does not suffer from the same steric repulsion as a diffusing polymer chain creating a brush-like polymer tethered on the surface but leads to a less homogeneous polymer layer. Asai et al.[21] observed that the grafting-to strategy leads to a more uniform polymer coverage of the NCs surface at a given grafting density. The main parameters that control the quality of the PGNs dispersion and the performance of the final nanocomposites have been the subject of many scientific works. Recently, Kumar et al.[22] demonstrated that the main parameters that control the dispersion of the PGNs are the molecular weight of the grafted chains and the polymer matrix (N, P respectively) together with the grafting density (σ), i.e., the number of chains per unit area of the nanoparticle. Homogeneous distribution of single PNGs requires a high molecular weight of the grafted chains (N) and/or high surface coverage (σ) together with polymer matrix with molecular weights (P) lower than that of the grafting chains.[23] A possible further improvement is the usage of mixed layers, with a mixture of short chains that cover the surface tightly, interspersed with a few longer chains, whose mushroom tops form a second protective layer around the particle. Benicewicz et al. showed in their works that densely grafted short brushes enthalpically screen the core/core attraction, and sparsely grafted long chains lower the entropic dewetting of high-molecular-weight polymer matrices and enhance the number of entanglements with the matrix.[24] In other words, they suggest that the best surface morphology that allows good dispersion of a nanosized inorganic particle in an organic matrix is the bimodal brush system. The peculiar behavior of having two different brushes on the surface of the nanoparticles was demonstrated experimentally in the case of gold nanoparticles,[25] zirconia,[26] and by coarse-grained simulations.[27]

Here, we report on the fabrication of polymer nanocomposites with increased refractive index based on a commercial thermoplastic polyurethane AG8451 by the addition of organophilic rodlike anatase nanocrystals (NCs). NCs (<15 nm) are obtained by colloidal synthesis in the presence of oleic acid as capping agent. The formation of a mixed double layer was done through the grafting-to approach with the introduction of an additional layer of poly(ethylene oxide) monomethyl ether (mPEO, M_W = 5000 g/mol). The presence of high loading of a low-dimensional anatase NCs, grafted with a single or mixed layer, into the TPU matrix produced an improvement of the nanocomposite mechanical properties and the enhancement of the refractive index, maintaining its clearness.

2. EXPERIMENTAL SECTION

2.1. Reagents. Titanium(IV) isopropoxide (TTIP, 99.999%), oleic acid (OLAC, 90%), oleyl amine (OLAM, 70%), trimethylamine N-oxide dihydrate (TMAO, 98%), triethylamine (TEA), phosphoryl chloride ($POCl_3$ >98%) freshly distilled before reactions, and tetrahydrofuran (THF >99%) dried with sodium wire and benzophenone and distilled before the reactions start were purchased from Sigma-Aldrich (Merck). Chloroform ($CHCl_3$), diethyl ether, and toluene (≥99.9%) are eventually dried over calcium chloride and distilled over activated molecular sieves. All solvents used were of analytical grade and purchased from Aldrich. Poly(ethylene oxide) monomethyl ether ($M\bar{w}$ = 5000 g/mol) was precipitated twice from ethanol, dried by azeotropic distillation from toluene, and stored in a dry nitrogen atmosphere. Polyurethane thermoplastic used is Estane AG8451, produced by Lubrizol. It is a polyether-based aliphatic (TPU) specifically designed for glass lamination with high optical transparency requirements, though AG8451 is an excellent general-purpose polymer for all optical applications where aliphatic polymers are required.

2.2. Synthesis of Anatase TiO_2 NCs. The synthetic method used is a modified version of the procedure proposed by Buonsanti et al.[28] OLAC (1.5 mol) is added in a round-bottom flask, previously dried. In order to work in an air-free environment, OLAC is first degassed with three vacuum/nitrogen cycles and further degassed at 120 °C for 2 h. The mixture is then cooled down to 90 °C under N_2 flow; when the target temperature is reached, TTIP (0.011 mol) is added in a single portion. After exactly 5 min, a solution of TMAO (0.0367 mol, 2 M) in water is injected in a single portion. The flask is heated up to 120 °C at a ramp rate of ∼25 °C/min and then left to react under vigorous stirring for 24 h. The solution turned from a clear, pale-yellow mixture to a milky solution. The crude product is then centrifuged, precipitating a white solid constituted by titania NCs covered by oleic acid. The particles are precipitated several times in ethanol to remove excess ligands and eventually dispersed in hexane, chloroform, or DCM.

2.3. Synthesis of mPEO Phosphate. mPEO (M_W = 5000 g/mol) is modified following the procedure proposed by Zalipsky.[29] Typically, mPEO (0.5 mmol) is dissolved in dry DCM and added dropwise to a solution of phosphoryl chloride ($POCl_3$, 1.2 equiv) and TEA (2.4 equiv) in an ice bath. The mixture was allowed to warm to room temperature and stirred for 24 h. Then, deionized water (5 mL) is slowly added to the mixture and allowed to react for 1 h. The solvent is dried in vacuum, and the crude product is dissolved in DCM and extracted with acidic water (HCl 0.2 mM) and then extracted three times with saturated brine. The organic phase is collected and dried over $MgSO_3$, filtered, and precipitated three times in diethyl ether. ^{1}H NMR (500 MHz, $CDCl_3$): 4.12 ppm (m, 2H, CH_2CH_2−O−P), δ 3.62 ppm (m, 454H, $-CH_2CH_2-$ PEO chain), δ 3.34 ppm (s, 3H, $-OCH_3$); ^{31}P NMR (500 MHz, $CDCl_3$): δ 2.01 ppm (s, 1P, $OP(OH)_2$).

2.4. Surface Modification of Anatase TiO_2 NCs. The grafting reaction is made with the phosphate-modified mPEO. The polymer is dissolved in $CHCl_3$ and the anatase NCs, dispersed in $CHCl_3$, are added to the solution, then the mixture is sonicated for 10 min before it is allowed to react for

https://doi.org/10.1021/acsomega.4c01053
ACS Omega 2024, 9, 29339−29349

16 h at reflux condition. The product is purified by ultracentrifugation with a mixture of chloroform diethyl ether 1:2.5 for at least three times (40 000 rcf). This process is a direct ligand exchange that provides a mixed bimodal system.

2.5. Kinetic Study of Surface Modification. The study of this process was made on the phosphate-modified mPEO. The amount of mPEO is 0.25 equiv with respect to the moles of OLAC (1.25 mol) present on the pristine NCs. The polymer is dissolved in $CHCl_3$ and the anatase NCs, also dispersed in $CHCl_3$, are added in the solution. Then, the mixture is sonicated for 10 min and then is left to react for 120 min at reflux condition. An amount of the crude solution is withdrawn every 20 min and purified as described before the analysis.

2.6. Nanocomposite Film Preparation. The film preparation is made through a solvent casting process. Two sets of samples have been prepared starting from different NCs, the first set using oleic acid capped anatase (OLAC@Anatase) and the second set with a mixed double layer made of mPEO and oleic acid (mPEO-OLAC@Anatase). In a standard procedure, the TPU is dissolved in chloroform at a concentration of 0.033 g/mL. A chloroform dispersion, 0.1 g/mL OLAC@Anatase or mPEO-OLAC@Anatase, is prepared and then added in a round-bottom flask alongside the dissolved TPU. The mixture is then brought to 70 mL of total volume and stirred overnight at 40 °C. The dispersion is poured in a Petri dish to slowly evaporate the solvent at room temperature, overnight. Once the solvent completely evaporates, a film is obtained and in order to get rid of defects is annealed for 12 h at 80 °C.

2.7. Characterization Methods. *2.7.1. Dynamic Light Scattering (DLS).* The hydrodynamic diameter and size distributions of the particles were determined by DLS in deionized water and DCM (0.1 mg/mL). The measures were recorded at 25 °C on a Malvern Zetasizer equipped with a continuous wave 1 mW He−Ne laser operating at 632.8 nm and an avalanche photodiode detector, Q.E. >50% at 633 nm, placed at 173° with respect to the incident beam. Reported data are the averages of at least three different measurements of the size distribution as a function of the intensity.

2.7.2. BET. Nitrogen adsorption−desorption isotherms were measured at liquid nitrogen temperature using an ASAP 2010 analyzer (Micromeritics). The samples were outgassed for 12 h at 473 K. The surface area was calculated by using the Brunauer−Emmet−Teller (BET) model.

2.7.3. XRD. For X-ray characterization, a D8 Advance powder diffractometer (Bruker) was used with Cu $K\alpha_1$ radiation (λ = 1.5418 Å) and a secondary-beam monochromator. The powder is added to a quartz sample holder and measured.

2.7.4. Attenuated Total Reflection (ATR)-FTIR. Fourier transform infrared characterization was performed by using a PerkinElmer spectrum 100 instrument scanning from 650 to 4000 cm^{-1} with a resolution of 4 cm^{-1} for 64 scans. The sample, in the form of powder, is added to the sample holder and directly analyzed over the Si crystal with the Universal ATR (UATR).

2.7.5. Thermogravimetric Analysis (TGA). Thermogravimetric analysis was carried out with a Mettler Toledo TGA/DSC1 STARe System at a constant gas flow (50 mL/min). The thermal profile was the following: 25 °C for 5 min (air); 25−800 °C with a rate of 10 °C/min (air).

2.7.6. Bright-Field Transmission Electron Microscopy (BF-TEM). TEM imaging was performed on a JEOL JEM-1220 microscope equipped with a thermionic gun operating at a 100 kV accelerating voltage. For these analyses, the samples were prepared by dropping dilute suspensions of NCs onto carbon-coated 200 mesh copper grids.

2.7.7. Nuclear Magnetic Resonance (NMR). ^{1}H, ^{31}P NMR spectra were recorded by using a Bruker AMX-500 spectrometer operating at 500 MHz. Solid-state ^{13}C NMR and HPDEC NMR experiments were performed at 75.5 MHz on a solid-state magic angle spinning Bruker Avance 300 at 25 °C. The spinning rate was set to 10 kHz for both experiments. HPDEC were usually recorded with 2048 scans using a recycle delay of 2 s.

2.7.8. Gel Permeation Chromatography (GPC). Molecular weight distributions and polydispersity indexes were determined by GPC using a WATER 1515 isocratic HPLC Pump, a WATER 2414 refractive index detector, and four Styragel columns (HR2, HR3, HR4, HR5). Samples were dissolved in THF, and their chromatograms were recorded with a flow of 1.0 mL/min at 35 °C.

2.7.9. Differential Scanning Calorimetry (DSC). Thermal properties were determined by DSC using a Mettler Toledo DSC1 instrument with a heating and cooling rate of 20 or 10 K/min under a nitrogen gas flow (80 mL/min). Typical samples consist of 6 mg of polymer film inserted in a 40 μL aluminum pan.

2.7.10. Mechanical Test. Tensile tests were performed on rectangular-shaped film slices of dimensions 65 mm long, 15 mm wide, and 0.20 mm thick using a mechanical testing machine Zwick 1445 with a load cell of 100 N. Experiments were carried out at room temperature with a test speed of 500 mm/min and a preload of 0.1 MPa. Tensile strength, elongation at break, and elastic modulus have been determined as averages of 8−9 independent drawing experiments performed at the same conditions following the ASTM D882 standard. All of the information and values have been obtained with the testXpert II software.

2.7.11. Refractometer. Refractive indices were measured using a Metricon 2010 prism coupling refractometer Metricon 2010 working at 633 nm with an uncertainty lower than 10^{-3}. We performed 5 measurements at different points of the same sample to check the homogeneity and to evaluate the mean value of the refractive index and standard errors.

2.7.12. Transmittance. Film transmittances from 350 to 800 nm have been collected at normal incidence using a Cary 80 spectrophotometer.

3. RESULTS AND DISCUSSION

In order to obtain a transparent nanocomposite, the inorganic filler must have a diameter under 50−60 nm to avoid the Rayleigh scattering of light, a phenomenon that determines an opaque appearance of the material.[14,30] A preliminary morphological study was done by TEM micrograph analysis (Figure 1) of the prepared NCs, where they appeared as rod-shaped NCs with a main axis of about 12 nm, a value confirmed also by XRD data presented in Figure 2.

These requirements are fulfilled by the colloidal anatase nanocrystals used in this work. The crystalline phase anatase was defined through the analysis of the XRD diffractogram (Figure 2). The diffraction peaks are very broad, but their positions correspond to the regions where the peaks of bulk anatase are predicted in Table 1. Moreover, the line width was

https://doi.org/10.1021/acsomega.4c01053
ACS Omega 2024, 9, 29339−29349

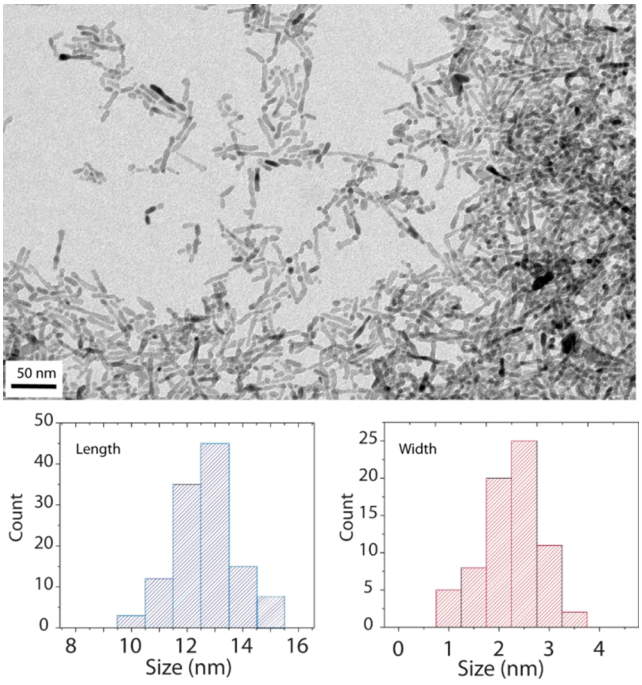

Figure 1. (Top) TEM image of colloidal anatase nanocrystals and (bottom) histograms related to the size distribution evaluated through the analysis of TEM pictures. (Bottom left) Length size distribution (blue pattern); (bottom right) width size distribution (red pattern).

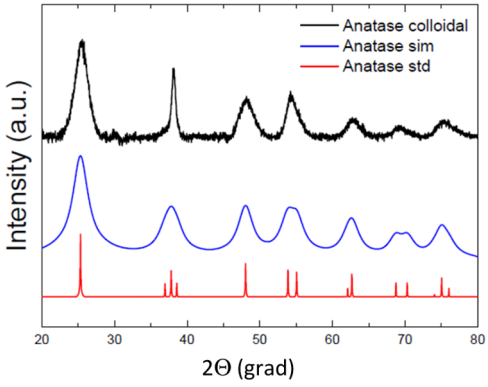

Figure 2. XRD pattern of the anatase colloidal NCs prepared by colloidal synthesis (top, black line); anatase nanocrystal simulated pattern (center, blue line), and anatase bulk standard (bottom, red line).

used to provide a second estimate of particle size as presented in Table 1. Rodlike NCs specific surface area was also calculated using a simple geometric model simplifying their shape into a cylinder capped with two semispheres. This value was compared with the one obtained performing N_2 adsorption showing good agreement (Table 1). The BET provides a global assessment of the exposed surface; its agreement with the data inferred from the size and shape of a single particle indicates that the absence of significant interparticle aggregation.[31]

To achieve complete transparency and to have an enhancement of properties, the filler must be well dispersed and distributed into the polymer matrix to avoid aggregation, which lowers the optical quality and the mechanical properties, of the final material. Therefore, the chemical structures of the polymeric materials used for the fabrication of the nanocomposite should be elucidated.

The commercial TPU used as a polymeric matrix was analyzed by GPC and NMR to understand its composition in order to properly engineer the inorganic surface. The molecular weight average of TPU is 58.6 kg/mol with a polydispersity index $Đ$ = 1.84 obtained by GPC. From the ^{1}H NMR spectrum, it is noted that the matrix is mainly constituted by aliphatic moieties and polyols (a mixture of polypropylene glycol, polybutanediol, polyoxymethylene, and a small amount of poly(ethylene glycol)) with no presence of aromatic groups (Figure 3).

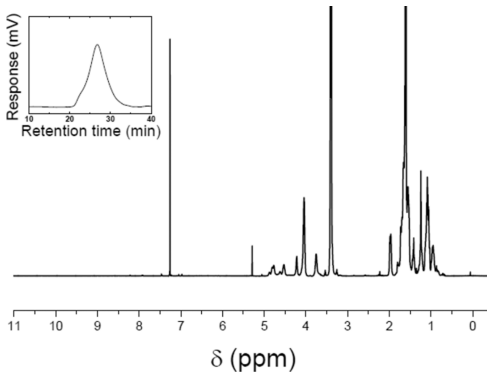

Figure 3. ^{1}H NMR spectra in $CDCl_3$ and (inset) GPC analysis of the AG8451 TPU matrix.

Since the PU matrix is found to be composed mainly of polyols and aliphatic chains, poly(ethylene oxide) monomethyl ether (mPEO) and OLAC would be good compatibilizers between the inorganic crystal and this polymer matrix. In order to test the behavior of this kind of system, two sets of samples have been prepared: one using only oleic acid-grafted nanocrystals and a second one with both OLAC and mPEO.

A prerequisite for filler particles is the actual presence of a compatibilizer on the surface. The presence of OLAC tied to the NCs surface (OLAC@Anatase) is detected with FTIR analysis (Figure 4). The weight percentage of OLAC is estimated by TGA, and the amount of organic ligand is approximately 27% of the total weight.

3.1. Mixed Double-Layer Synthesis and Characterization. Fatty acids are weakly bonded to inorganic surfaces

Table 1. Crystal Dimensions of OLAC@Anatase Derived from XRD Calculated at 38.2° (004) peak, TEM Micrographs, and DLS Measured in Hexane Reported with Its PDI[a]

	XRD		TEM		DLS		SSA_{exp}		$SSA_{predicted}$	
sample	nm	std. dev.	nm	std. dev.	nm	PDI	$m^2\ g^{-1}$	std. dev.	$m^2\ g^{-1}$	std. dev.
anatase	10.9	0.4	12.3	1.1	15.9	0.157	200	7	229	32

[a]Experimental specific surface area (SSA_{exp}) from nitrogen adsorption as well as an estimate of surface area based on TEM size and calculated using the Sauter equation ($SSA_{predicted}$).

https://doi.org/10.1021/acsomega.4c01053
ACS Omega 2024, 9, 29339−29349

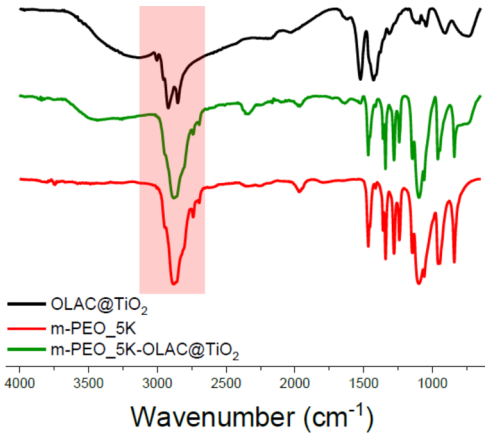

Figure 4. FTIR (top to bottom): OLAC@Anatase black line; mPEO_5K-OLAC@Anatase green line, mPEO_5K red line and red region. The highlighted region indicates the vibrational peak of the mPEO chains at 2900 cm^{-1}.

and are usually replaced with a silane agent and a phosphonic acid/phosphate moiety to obtain stronger binding. The bimodal systems were obtained with a direct ligand exchange between the OLAC and mPEO functionalized with a phosphate end group.[32] The yield of the exchange process has been verified qualitatively through DLS, FTIR, and ^{13}C SS NMR, while ^{1}H NMR and TGA were used for quantitation. From the comparison between the FTIR spectra (Figure 4) of OLAC@Anatase with the phosphate mPEO (mPEO_5K) and the mixed double layer (mPEO_5K-OLAC@Anatase), it is possible to detect the characteristic vibrational peaks of the mPEO chains. The sample mPEO_5K-OLAC@Anatase has a vibration peak at 2900 cm^{-1} related to the stretching of the CH_2 groups and at 1100 cm^{-1} the C−O bond vibration peak. The peaks related to the presence of OLAC are detected at 1520 and 1410 cm^{-1}.

To get a better picture of the mixed double-layer samples, high-power decoupling (HP-DEC) solid-state ^{13}C NMR analysis is performed (Figure 5).[33] In the OLAC@Anatase spectrum, the peak at 15 ppm is related to the methyl end group of the aliphatic chain, the peaks between 25 and 38 ppm are related to the carbons of the aliphatic chains, and the peak

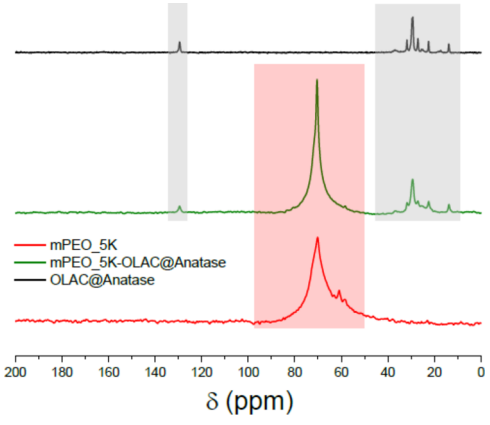

Figure 5. HP-DEC ^{13}C MAS NMR, recycle delay 2 s, and spin rate 10 kHz. Top to bottom: OLAC@Anatase black line with the characteristic peaks in the gray region; mPEO_5K-OLAC@Anatase green line, mPEO_5K red line and red region.

at 130 ppm is related to the carbons of the double bond. The peak at 180 ppm related to the C═O bond is missing due to the low mobility of this group since it is attached on the surface.[34] In the mPEO_5K spectrum is present at 70.2 ppm the peak of the carbons that belong to the polymeric chain.[35] The spectra of the mPEO_5K-OLAC@Anatase are the sum of the previously described samples, confirming the presence of both OLAC and mPEO.

DLS measures of the hydrodynamic diameter (d_h) of the pristine NCs and the mixed double-layer NCs are reported in Figure 6. The d_h of the OLAC grafted NC is 15.9 ± 6 nm with

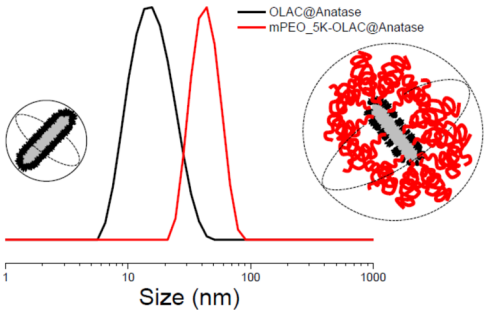

Figure 6. DLS measured in chloroform of the pristine NCs (OLAC@Anatase, black line) and the mixed double-layer NCs (mPEO_5K-OLAC@Anatase, red line).

a polydispersity index (PDI) equal to 0.222, while the polymer-grafted NC has a d_h of 43.8 ± 11 nm with a PDI equal to 0.168. The DLS analysis shows an increase of the size of the mPEO-OLAC@Anatase due to the larger dimension of the grafted polymer. The presence of this polymer layer enables a better size distribution and stability highlighted by the lower PDI value.

A set of experiments were made to study the kinetics of the exchange process following the experimental protocol described in Section 2. The graft density is calculated from the TGA and BET data (Table 2), whereas the composition of the brush is obtained from the integration of the ^{1}H NMR spectra. As clearly visible from the spectrum of mPEO_5K-OLAC@Anatase reported in Figure 7, the triplet at 0.88 ppm is attributed to the $-CH_3$ end group of OLAC and the complex signals that lie in the 1.5−1.20 ppm region are generated by the protons of the aliphatic chains that do not belong to the two double bonded carbons. At 3.37 ppm, the triplet is found attributed to the $-CH_3$ end group of mPEO, while the region between 3.9 and 3.4 ppm belongs to the 454 protons of the mPEO chain.[36] The molar fraction (f) of mPEO is calculated using the integral of the mPEO protons as an internal reference. It is assigned a value of 457, which corresponds to the number of protons of a single mPEO chain. The integral of the OLAC protons in the region between 1.5 and 0.7 ppm divided by the 31 protons of a single OLAC molecule defines the number of OLAC molecules for each mPEO chain. This number provides the molar ratio between the two populations of tethered molecules on the anatase surface.

Data show that the PEO fraction reaches a plateau of 23% around 100−120 min. It seems that PEO chains are not able to substitute all of the OLAC moieties on the titania surface. PEO with a molecular weight of 5000 Da has, in water, a radius of gyration of 4.3 nm, instead OLEAC is significantly smaller, and a brush height of 2 nm was measured for OLEAC on iron

https://doi.org/10.1021/acsomega.4c01053
ACS Omega 2024, 9, 29339−29349

Table 2. Experimental Data of the Molar Fraction Calculated from TGA[a]

				σ_{mPEO_5K}		σ_{OLAC}	
sample	$W_{total\ loss}$ (%)	f_{mPEO_5K} (%)	f_{OLAC} (%)	ch nm^{-2}	std. dev.	ch nm^{-2}	std. dev.
t = 5	77.59	0.17	0.83	0.69	0.04	3.26	0.04
t = 20	77.55	0.18	0.82	0.70	0.04	3.24	0.04
t = 40	79.76	0.19	0.81	0.84	0.04	3.65	0.04
t = 60	82.17	0.20	0.80	1.03	0.05	4.22	0.04
t = 80	79.46	0.21	0.79	0.92	0.04	3.49	0.04
t = 100	78.94	0.23	0.77	0.97	0.04	3.31	0.04
t = 120	76.39	0.23	0.77	0.86	0.04	2.83	0.04

[a] f_{mPEO_5K}, molar fraction of the polymer; f_{OLAC}, molar fraction of the oleic acid; σ_{mPEO_5K}, extrapolated graft density of mPEO_5K; and σ_{OLAC}, extrapolated graft density of oleic acid. The reaction was carried out starting with mPEO_5K/OLAC = 0.25:1 molar ratio.

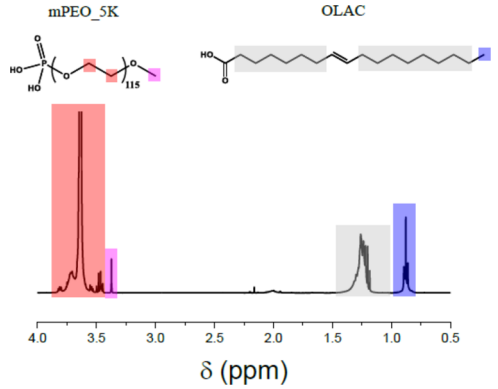

Figure 7. ^{1}H NMR spectra of mPEO_5K-OLAC@Anatase in $CDCl_3$; the mPEO phosphate molecule and the OLAC structure are represented.

oxide.[37] This difference in size and the higher conformational freedom of PEO can explain the fact that a large part of OLAC is not substituted by PEO. Most probably when a molecule of PEO substitutes one of OLAC, it changes its conformation close to the surface in order to fit in the space left empty, but the remaining part of the chain forms a mushroom top that screens the next neighbor OLAC molecules that become sterically inaccessible.

3.2. High Refractive TPU@TiO_2 Nanocomposites. Two series of TPU-based nanocomposite films containing NCs have been prepared with a solvent casting technique: one containing OLAC@Anatase NCs, the other the double-brush Anatase NCs (f_{mPEO_5K}/f_{OLAC} = 1:4). All of the films appear transparent and slightly colored as the inorganic loading increases (Figure 8). The homogeneous dispersion of the titania NC is confirmed by the TEM images of the OLAC@Anatase/TPU 50 wt % nanocomposite,[38] where the NCs are clearly visible with dimensions and shape analogous to those of the pristine powder (see the Supporting Information). Since both TPU and TiO_2 have no significant absorption in the visible range, the origin of the optical losses is related to the size of the filler, which produces a Rayleigh scattering effect on the bulk material. This is confirmed by the optical transmission of the nanocomposites (Figure 8). The pristine TPU sample shows a transmittance in the high-wavelength region of about 91%. This value corresponds to the expected Fresnel reflection losses due to the difference in refractive indices between the air and the film, which in our case, for n_{PTU} = 1.49, is around 8%. Fresnel losses are of the same order also for the sample loaded with 15% TiO_2 in weight. Therefore, in the absence of scattering losses, the loaded sample should have a similar transmittance spectrum with respect to that of the pristine sample. On the contrary, the optical transmission spectra show losses well above 9%. These excesses are entirely due to Rayleigh scattering. The fact that even the OLAC@Anatase is well dispersed is due to the highly aliphatic content of the TPU used. Not only the graft density and the NCs ligand architecture affect the dispersibility but also the chemical affinity between the organic matrix and the NCs ligand.

The films were characterized with TGA to check the correct composition of all of the samples. The first derivative of TGA of neat TPU presents two main peaks related to the polymer decomposition. As the inorganic lading increases, there is a decrease of the intensity of TPU peaks and the decomposition peak of the mPEO appears (Figure 9).

A series of tensile tests were performed to determine the mechanical behavior of the nanocomposites. Neat TPU is used as a reference. The results are compared between films prepared from NCs functionalized with a mixed double layer and NCs covered with a single layer of OLAC. Once the films have been annealed and peeled from the glass substrate, they have been cut into 9 slices and characterized. Elastic modulus and elongation at break, Table 3 and Figure 10, have been determined as averages of nine independent drawing performed at the same conditions following the ASTM D882 standard.

Nanocomposite films show a significant increase of the elastic modulus as a function of titania content; at the same time, elongation at break decreases considerably. At high titania loading, the nanocomposite becomes hard and stiff. As reported above, very few studies deal with TiO_2 NC dispersed in TPU matrices. Nayak and co-workers report about PU nanocomposites obtained by mixing a polyester polyurethane and ball-milled anatase (average particle size found through DLS was close to 250 nm),[39] the content of TiO_2 ranged from 23 to 47 wt %. The tensile strength increased a little for composites containing 23 wt %, instead the tensile strength decreased with a further increase in titania loading. The authors attribute this behavior to filler aggregating tendency, and filler particles are not properly wetted by the polymer matrix since they use bare titania particles (i.e., filler particles are not attached to polymer chains). In the case of OLAC@Anatase and mPEO_5K-OLAC@Anatase, instead a significant wetting is present, and eventually mPEO_5K chains can entangle with PU macromolecules. At equal anatase loading, the presence of a double layer with a polymer increases the elastic modulus more than that of a single layer. As expected, for both samples, the elongation at break decreases as the inorganic loading increases. In the case of the mixed double-layer nanocomposite, the elongation at break is lower than in

https://doi.org/10.1021/acsomega.4c01053
ACS Omega 2024, 9, 29339−29349

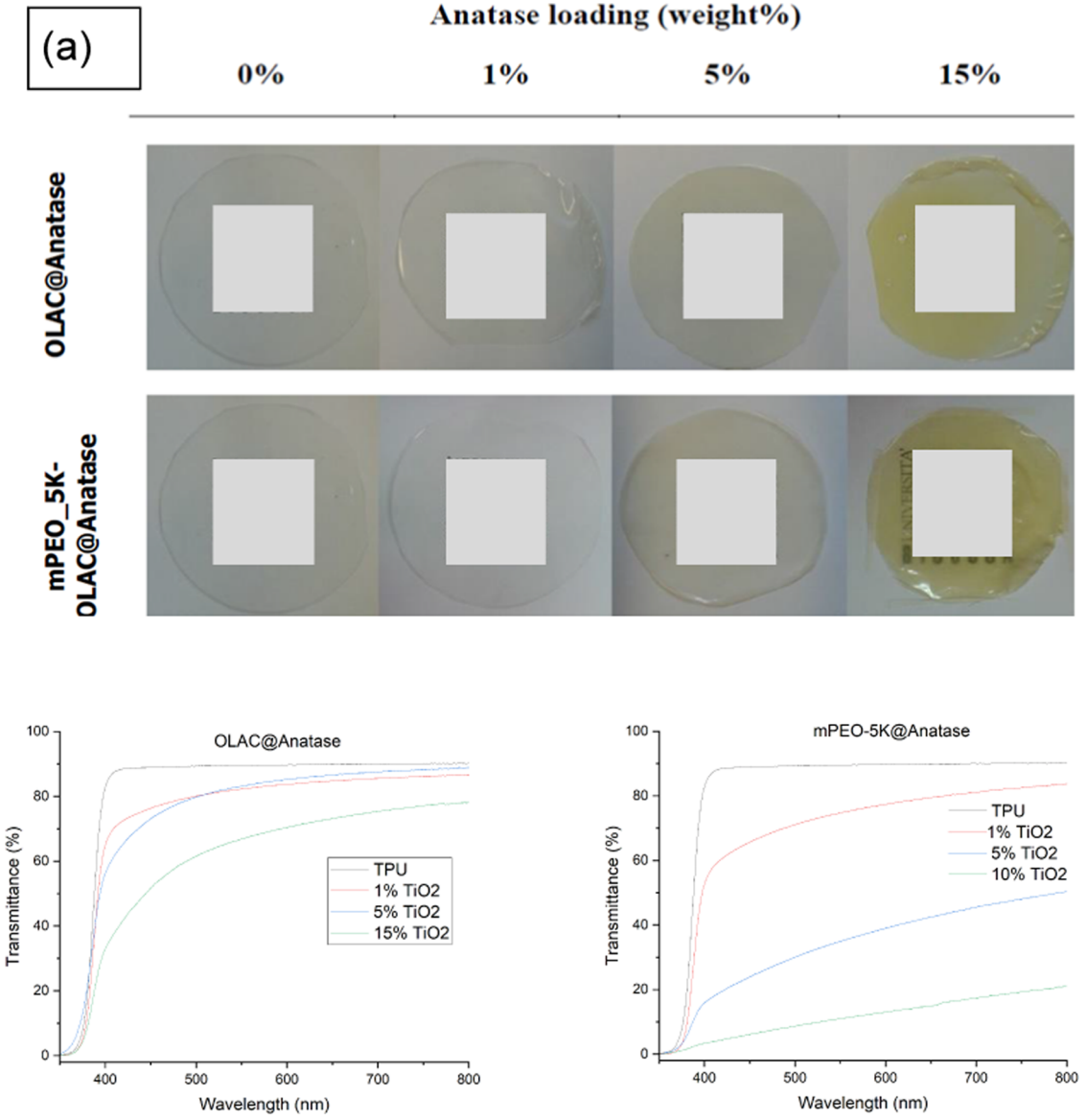

Figure 8. Top: pictures of the TPU-based nanocomposite films. Bottom: optical transmission of the nanocomposites.

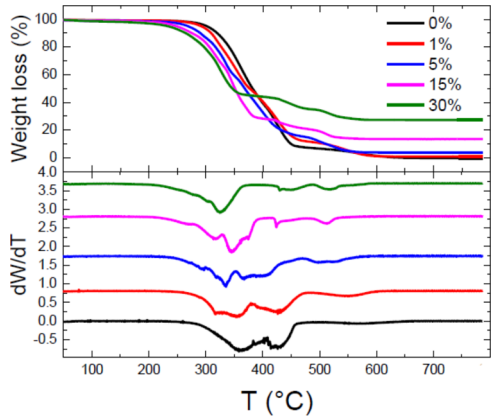

Figure 9. TGA of mPEO_5K-OLAC@Anatase with increased anatase loading. The top graph refers to the thermogravimetric curve; the bottom graph refers to the first derivative of weight loss function of temperature.

the single-layer samples. This phenomenon is the effect of the presence of a rigid object inside the polymer matrix, which leads to poorer elastic behavior. Moreover, the polymer grafted onto the NCs is able to form a greater number of entanglements with the TPU polymer matrix, resulting in a tougher and more fragile material. This phenomenon can explain the fact that for concentrations higher than 15 wt % of mPEO_5K-OLAC@Anatase nanoparticles in PU, it was not possible to recover intact films due to the brittleness of the nanocomposites. On the other hand, for OLAC@Anatase nanoparticles, cohesive and transparent films could be retrieved even for 37.5 wt % of filler content. A nanocomposite containing 50 wt % was also prepared, but it was too brittle for measuring the tensile properties.

3.3. Optical Properties Analysis. The total refractive index of a multicomponent material is proportional to the volume fraction of the different components. The challenge is to produce a bulk material that is highly loaded with titanium dioxide that maintains its transparency and clearness in all visible spectrum. The transparency is achieved by avoiding any

https://doi.org/10.1021/acsomega.4c01053
ACS Omega 2024, 9, 29339−29349

Table 3. Mechanical Properties of the Titania/PU Nanocomposites[a]

	mPEO_5K-OLAC@anatase				OLAC@anatase			
TiO_2 weight (%)	elastic modulus (MPa)	std. dev.	deformation at break (%)	std. dev.	elastic modulus (MPa)	std. dev.	deformation at break (%)	std. dev.
0	12.4	0.372	412.4	30.4	12.4	0.327	412.4	30.4
1	10.9	0.815	355.8	24	13.3	0.476	339.2	57.7
5	22.7	0.686	262.2	13	16.3	0.683	349.1	48.2
10	31	4	286	18.2				
15	39.8	5.62	290.2	33.4	30.1	1.48	372	76.1
25					76.7	5.68	323.5	51.1
30					152.3	15.6	20	4.1
37.5					223	29.1	18.8	5.6

[a]The data are averaged from a set of 9 experiments; all of the results are reported with their standard deviation.

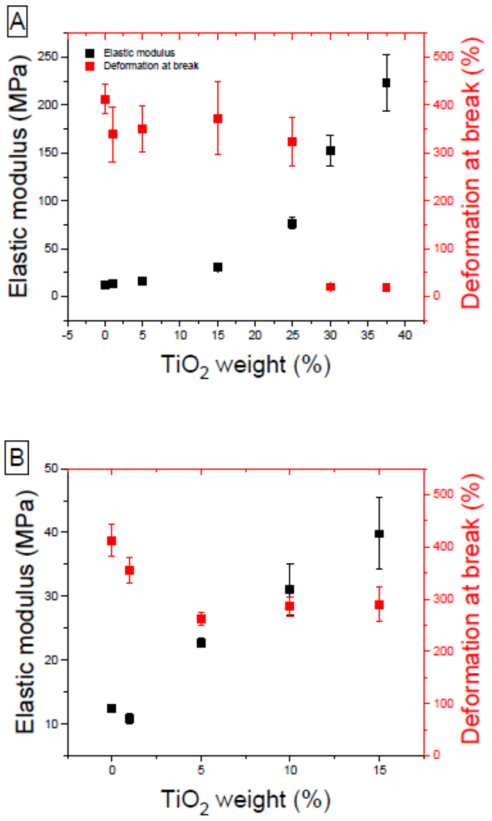

Figure 10. Elastic modulus (black squares) and deformation at break (red square) as a function of the anatase wt % loading. (A) Results of samples with OLAC@Anatase; (B) samples with mPEO_5K-OLAC@Anatase.

aggregation of the inorganic filler, which is possible with a fine-tuning of the surface chemistry. In order to measure the refractive index of the TPU-based nanocomposite material, a prism coupling refractometer was used working at 633 nm. Measurements were performed at five different points of the same sample to check the homogeneity. The refractive index n is theoretically described by eq 1

$$n_{\text{composite}} = \sum_{i=1}^{n} n_i \cdot \phi_i \quad (1)$$

where n_i represents the refractive index of the ith component and ϕ_i represents the volume fraction of the ith component. In Tables 4 and 5, the refractive indices of the single-brush OLAC@Anatase and double-brush mPEO_5K-OLAC@Anatase samples are reported respectively.

Table 4. Refractive Index Results of the OLAC@Anatase Samples[a]

W_{anatase} (%)	Φ_{anatase} (%)	Φ_{OLAC} (%)	Φ_{TPU} (%)	$n_{\text{theoretical}}$	$n_{\text{experimental}}$	std. dev.
0	0.0	0.0	100.0	1.4962	1.4980	0.0002
1	0.3	0.6	99.1	1.4988	1.5012	0.0002
5	1.4	1.9	96.7	1.5102	1.5087	0.0001
15	4.6	6.7	88.7	1.5409	1.5295	0.0001
25	8.3	12.3	79.5	1.5763	1.5684	0.0006
30	10.9	15.9	73.2	1.6016	1.5906	0.0012
37.5	13.8	20.0	66.3	1.6296	1.6114	0.0002
50	20.6	29.7	49.7	1.6964	1.6533	0.0018

[a]ϕ_{anatase}, ϕ_{OLAC}, and ϕ_{TPU} represent the volume fractions; n represents the refractive index; theoretical values calculated with eq 1 and the experimental values with their standard deviation are reported.

The refractive index of the nanocomposite materials containing single-brush titania NCs increases proportionally from 1.49 to 1.65 as the volume fraction of titanium dioxide increases (Figure 11A).

Analogous results for similar titania contents are reported by Tao et al. for composites obtained by poly(glycidyl methacrylate) (PGMA) polymer chains grafted on titania nanoparticles through an alkyne−azide "'click'" reaction.[40] The linear dependence of the refractive index in composite materials with filler loading has been reported from both experimental measurements and theoretical calculations. The extrapolated refractive index of the anatase nanocrystals from linear approximation to 100% TiO_2 content was 2.35, which is close to the reported index of 2.45 for anatase phase TiO_2 nanoparticles at 633 nm wavelength.

In the case of NCs with a double brush of oleic acid and PEO molecules, a similar behavior is found, although films become brittle, exceeding 15% by weight of titania in the composite (Table 5 and Figure 11B).

The linear dependence of the refractive index was predicted for homogeneously dispersed nanofillers within a matrix. The good linear fitting of the refractive index of TiO_2 nanocomposites indicates that excellent dispersion of particles is achieved. It is worth mentioning that reaching high transparency only through refractive index matching is very challenging, and controlling the dispersion of nanoparticles within the polymer matrix is even more critical. Even with a small refractive index mismatch, the transparency degrades

https://doi.org/10.1021/acsomega.4c01053
ACS Omega 2024, 9, 29339−29349

Table 5. Refractive Index Results of the mPEO_5K-OLAC@Anatase Samples[a]

$W_{anatase}$ (%)	$\Phi_{anatase}$ (%)	Φ_{mPEO_5K} (%)	Φ_{OLAC} (%)	Φ_{TPU} (%)	$n_{theoretical}$	$n_{experimental}$	std. dev.
0	0.0	0.0	0.0	100	1.4962	1.4980	0.0002
1	0.3	2.5	0.4	96.9	1.4980	1.4979	0.0002
5	1.4	14.0	1.9	82.7	1.5057	1.5082	0.0005
10	1.8	17.6	2.4	78.2	1.5137	1.5126	0.0003
15	4.6	32.1	4.3	59.0	1.5329	1.5300	0.0010

[a]$\Phi_{anatase}$, Φ_{mPEO_5K}, Φ_{OLAC}, and Φ_{TPU} represent the volume fraction; n represents the refractive index; theoretical values calculated with eq 1 and the experimental values with their std. dev. are reported

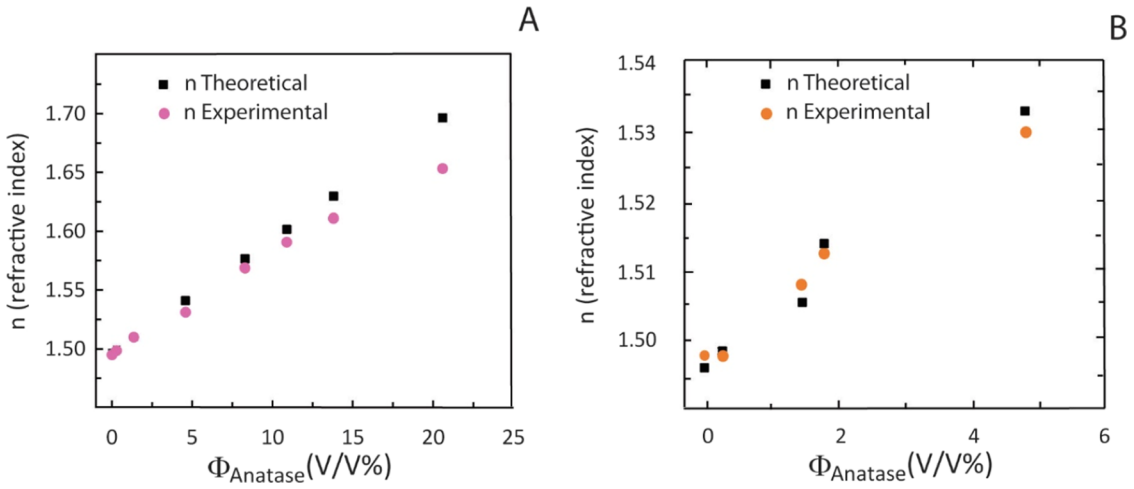

Figure 11. n theoretical (black squares) and experimental (magenta and orange circles) as a function of anatase volume fraction (ϕ). (A) Results of the OLAC@Anatase in TPU matrix; (B) results of the mPEO_5K-OLAC@Anatase in TPU matrix.

rapidly with increased solid loading. Despite the large mismatch of refractive index ($\Delta n \approx 1$) between the titania nanocrystals and the organic polymer, transparent nanocomposites were prepared. The fact that even with a single OLAC layer transparent films are produced is evidence of the excellent chemical affinity between the highly aliphatic TPU and the prepared NCs. As discussed in the Introduction section, several polymer nanocomposites with increased refractive index as a function of nanofiller content are reported in the literature; however, very few examples are reported for TPU. Ireni and co-workers report a TPU/TiO_2 transparent nanocomposite with a maximum increase $\Delta n = 0.036$ at 5 wt % of titania nanoparticles,[41] to be compared to $\Delta n = 0.1131$ at 37.5 wt % of OLAC@Anatase NC.

4. CONCLUSIONS

In this work, we prepared a highly loaded TPU-based nanocomposite material with a facile and scalable casting process. The NCs synthesis produced low-dimensional anatase TiO_2 NCs capped with OLAC that have been subsequently exchanged with mPEO. The obtained NCs have been used to produce transparent nanocomposites with high refractive index and with improved mechanical properties. The refractive index of the composites increased by 10.4% with 50 wt % loading of TiO_2 fillers, while the film transparency was maintained. The mixed double layer and single layer effectively screen TiO_2 nanoparticles from forming agglomerated TPU nanocomposites with a high content of inorganic particles, minimizing transparency loss due to scattering. Moreover, the elastic modulus of the as-prepared materials increases up to 223 MPa for the sample loaded with OLAC@Anatase at 37.5 wt % anatase, with respect to 12.4 MPa of neat TPU film. The mixed double-layer grafted NCs, at equal titanium dioxide loading, showed better mechanical properties than the samples covered by only OLAC. Functionalizing polymer chains onto the surface of high-refractive-index inorganic nanoparticles is a simple and effective way to achieve excellent dispersion of nanoparticles, even at high loading levels, and to fabricate transparent, high-refractive-index polymer nanocomposites with improved mechanical properties.

■ ASSOCIATED CONTENT

Supporting Information

The Supporting Information is available free of charge at https://pubs.acs.org/doi/10.1021/acsomega.4c01053.

Experimental details and protocol for the sample preparation for TEM and TEM images (PDF)

■ AUTHOR INFORMATION

Corresponding Author

Roberto Simonutti − *Department of Materials Science, University of Milano-Bicocca, 20125 Milano, Italy;* orcid.org/0000-0001-8093-517X; Email: roberto.simonutti@unimib.it

Authors

Massimo Tawfilas − *Department of Materials Science, University of Milano-Bicocca, 20125 Milano, Italy*

Gianluca Bartolini Torres − *Department of Materials Science, University of Milano-Bicocca, 20125 Milano, Italy*

Roberto Lorenzi − *Department of Materials Science, University of Milano-Bicocca, 20125 Milano, Italy;* orcid.org/0000-0002-6199-0971

https://doi.org/10.1021/acsomega.4c01053
ACS Omega 2024, 9, 29339−29349

Melissa Saibene − *Piattaforma di Microscopia, University of Milano-Bicocca, 20126 Milano, Italy*
Michele Mauri − *Department of Materials Science, University of Milano-Bicocca, 20125 Milano, Italy;* orcid.org/0000-0002-7777-9820

Complete contact information is available at: https://pubs.acs.org/10.1021/acsomega.4c01053

Notes

The authors declare no competing financial interest.

■ ACKNOWLEDGMENTS

The authors thank Dr. Alberto Bianchi for helpful discussions.

■ REFERENCES

(1) (a) Spontak, R. J.; Patel, N. P. Thermoplastic elastomers: fundamentals and applications. *Curr. Opin. Colloid Interface Sci.* **2000**, *5* (5−6), 334−341. (b) Wang, W. Y.; Lu, W.; Goodwin, A.; Wang, H. Q.; Yin, P. C.; Kang, N. G.; Hong, K. L.; Mays, J. W. Recent advances in thermoplastic elastomers from living polymerizations: Macromolecular architectures and supramolecular chemistry. *Prog. Polym. Sci.* **2019**, *95*, 1−31.
(2) Akindoyo, J. O.; Beg, M. D. H.; Ghazali, S.; Islam, M. R.; Jeyaratnam, N.; Yuvaraj, A. R. Polyurethane types, synthesis and applications - a review. *RSC Adv.* **2016**, *6* (115), 114453−114482.
(3) Datta, J.; Kasprzyk, P. Thermoplastic polyurethanes derived from petrochemical or renewable resources: A comprehensive review. *Polym. Eng. Sci.* **2018**, *58*, E14−E35.
(4) Higashihara, T.; Ueda, M. Recent Progress in High Refractive Index Polymers. *Macromolecules* **2015**, *48* (7), 1915−1929.
(5) Xue, S. Y.; Lei, X. F.; Xiao, Y. Y.; Liu, Y.; Zhang, Y. X.; Zhang, Q. Y. Rapid, Mild Synthesis of Transparent Polyimides with High Refractive Index via Thiol-Michael Click Reaction. *ACS Appl. Polym. Mater.* **2024**, *6*, 2315−2326.
(6) Mazumder, K.; Voit, B.; Banerjee, S. Recent Progress in Sulfur-Containing High Refractive Index Polymers for Optical Applications. *ACS Omega* **2024**, *9*, 6253−6279.
(7) Loste, J.; Lopez-Cuesta, J. M.; Billon, L.; Garay, H.; Save, M. Transparent polymer nanocomposites: An overview on their synthesis and advanced properties. *Prog. Polym. Sci.* **2019**, *89*, 133−158.
(8) Giovino, M.; Pribyl, J.; Benicewicz, B.; Bucinell, R.; Schadler, L. Mechanical properties of polymer grafted nanoparticle composites. *Nanocomposites* **2018**, *4* (4), 244−252.
(9) (a) Althues, H.; Henle, J.; Kaskel, S. Functional inorganic nanofillers for transparent polymers. *Chem. Soc. Rev.* **2007**, *36* (9), 1454−1465. (b) Colombo, A.; Tassone, F.; Mauri, M.; Salerno, D.; Delaney, J. K.; Palmer, M. R.; De La Rie, R.; Simonutti, R. Highly transparent nanocomposite films from water-based poly(2-ethyl-2-oxazoline)/TiO2 dispersions. *RSC Adv.* **2012**, *2* (16), 6628−6636.
(10) Lü, C.; Yang, B. High refractive index organic-inorganic nanocomposites: design, synthesis and application. *J. Mater. Chem.* **2009**, *19* (19), 2884−2901.
(11) Cargnello, M.; Gordon, T. R.; Murray, C. B. Solution-Phase Synthesis of Titanium Dioxide Nanoparticles and Nanocrystals. *Chem. Rev.* **2014**, *114* (19), 9319−9345.
(12) Gnanaseelan, M.; Kalita, U.; Janke, A.; Pionteck, J.; Voit, B.; Singha, N. K. All methacrylate block copolymer/TiO_2 nanocomposite via ATRP and *in-situ* sol-gel process. *Mater. Today Commun.* **2020**, *22*, No. 100728.
(13) Mazumder, K.; Bittrich, E.; Voit, B.; Banerjee, S. Sulfur-Rich Polyimide/TiO_2 Hybrid Materials with a Tunable Refractive Index. *ACS Omega* **2023**, *8*, 43236−43242.
(14) Colombo, A.; Tassone, F.; Santolini, F.; Contiello, N.; Gambirasio, A.; Simonutti, R. Nanoparticle-doped large area PMMA plates with controlled optical diffusion. *J. Mater. Chem. C* **2013**, *1* (16), 2927−2934.
(15) He, X. L.; Pu, Y.; Wang, J. X.; Wang, D.; Chen, J. F. Surface Engineering of Titanium Dioxide Nanoparticles for Silicone-Based Transparent Hybrid Films with Ultrahigh Refractive Indexes. *Langmuir* **2021**, *37*, 2707−2713.
(16) Hore, M. J. A.; Korley, L. T. J.; Kumar, S. K. Polymer-Grafted Nanoparticles. *J. Appl. Phys.* **2020**, *128* (3), No. 030401.
(17) Ligoure, C.; Leibler, L. Thermodynamics and kinetics of grafting end-functionalized polymer to an interface. *J. Phys.* **1990**, *51* (12), 1313−1328.
(18) Labouta, H. I.; Gomez-Garcia, M. J.; Sarsons, C. D.; Nguyen, T.; Kennard, J.; Ngo, W.; Terefe, K.; Iragorri, N.; Lai, P.; Rinker, K. D.; Cramb, D. T. Surface-grafted polyethylene glycol conformation impacts the transport of PEG-functionalized liposomes through a tumour extracellular matrix model. *RSC Adv.* **2018**, *8* (14), 7697−7708.
(19) Abbas, Z. M.; Tawfilas, M.; Khani, M. M.; Golian, K.; Marsh, Z. M.; Jhalaria, M.; Simonutti, R.; Stefik, M.; Kumar, S. K.; Benicewicz, B. C. Reinforcement of polychloroprene by grafted silica nanoparticles. *Polymer* **2019**, *171*, 96−105.
(20) Paniagua, S. A.; Kim, Y.; Henry, K.; Kumar, R.; Perry, J. W.; Marder, S. R. Surface-Initiated Polymerization from Barium Titanate Nanoparticles for Hybrid Dielectric Capacitors. *ACS Appl. Mater. Interfaces* **2014**, *6* (5), 3477−3482.
(21) Asai, M.; Zhao, D.; Kumar, S. K. Role of Grafting Mechanism on the Polymer Coverage and Self-Assembly of Hairy Nanoparticles. *ACS Nano* **2017**, *11* (7), 7028−7035.
(22) Kumar, S. K.; Jouault, N.; Benicewicz, B.; Neely, T. Nanocomposites with Polymer Grafted Nanoparticles. *Macromolecules* **2013**, *46* (9), 3199−3214.
(23) Kumar, S. K.; Benicewicz, B. C.; Vaia, R. A.; Winey, K. I. 50th Anniversary Perspective: Are Polymer Nanocomposites Practical for Applications? *Macromolecules* **2017**, *50* (3), 714−731.
(24) Li, Y.; Krentz, T. M.; Wang, L.; Benicewicz, B. C.; Schadler, L. S. Ligand Engineering of Polymer Nanocomposites: From the Simple to the Complex. *ACS Appl. Mater. Interfaces* **2014**, *6* (9), 6005−6021.
(25) Moffitt, M. G. Self-Assembly of Polymer Brush-Functionalized Inorganic Nanoparticles: From Hairy Balls to Smart Molecular Mimics. *J. Phys. Chem. Lett.* **2013**, *4* (21), 3654−3666.
(26) Guzman-Juarez, B.; Abdelaal, A.; Kim, K.; Toader, V.; Reven, L. Fabrication of Amphiphilic Nanoparticles via Mixed Homopolymer Brushes and NMR Characterization of Surface Phase Separation. *Macromolecules* **2018**, *51* (23), 9951−9960.
(27) Koski, J. P.; Frischknecht, A. L. Self-Assembled Vesicles from Mixed Brush Nanoparticles in Solution. *Macromolecules* **2021**, *54* (11), 5144−5154.
(28) Buonsanti, R.; Grillo, V.; Carlino, E.; Giannini, C.; Kipp, T.; Cingolani, R.; Cozzoli, P. D. Nonhydrolytic synthesis of high-quality anisotropically shaped brookite TiO(2) nanocrystals. *J. Am. Chem. Soc.* **2008**, *130* (33), 11223−11233.
(29) Zalipsky, S. Functionalized poly(ethylene glycol) for preparation of biologically relevant conjugates. *Bioconjugate Chem.* **1995**, *6* (2), 150−165.
(30) Nakayama, N.; Hayashi, T. Preparation and characterization of TiO2 and polymer nanocomposite films with high refractive index. *J. Appl. Polym. Sci.* **2007**, *105* (6), 3662−3672.
(31) Tawfilas, M.; Mauri, M.; De Trizio, L.; Lorenzi, R.; Simonutti, R. Surface Characterization of TiO2 Polymorphic Nanocrystals through H-1-TD-NMR. *Langmuir* **2018**, *34* (32), 9460−9469.
(32) Mezzomo, L.; Lorenzi, R.; Mauri, M.; Simonutti, R.; D'Arienzo, M.; Wi, T.-U.; Ko, S.; Lee, H.-W.; Poggini, L.; Caneschi, A.; Mustarelli, P.; Ruffo, R. Unveiling the Role of PEO-Capped TiO2 Nanofiller in Stabilizing the Anode Interface in Lithium Metal Batteries. *Nano Lett.* **2022**, *22* (21), 8509−8518.
(33) (a) Laws, D. D.; Bitter, H. M. L.; Jerschow, A. Solid-state NMR spectroscopic methods in chemistry. *Angew. Chem., Int. Ed.* **2002**, *41* (17), 3096−3129. (b) Mauri, M.; Floudas, G.; Simonutti, R. Local Order and Dynamics of Nanoconstrained Ethylene-Butylene Chain Segments in SEBS. *Polymers* **2018**, *10* (6), No. 655.

(34) Simonutti, R.; Comotti, A.; Bracco, S.; Sozzani, P. Surfactant organization in MCM-41 mesoporous materials as studied by C-13 and Si-29 solid-state NMR. *Chem. Mater.* **2001**, *13* (3), 771−777.
(35) Selli, D.; Tawfilas, M.; Mauri, M.; Simonutti, R.; Di Valentin, C. Optimizing PEGylation of TiO2 Nanocrystals through a Combined Experimental and Computational Study. *Chem. Mater.* **2019**, *31* (18), 7531−7546.
(36) De Roo, J.; Yazdani, N.; Drijvers, E.; Lauria, A.; Maes, J.; Owen, J. S.; Van Driessche, I.; Niederberger, M.; Wood, V.; Martins, J. C.; Infante, I.; Hens, Z. Probing Solvent-Ligand Interactions in Colloidal Nanocrystals by the NMR Line Broadening. *Chem. Mater.* **2018**, *30* (15), 5485−5492.
(37) Doig, M.; Warrens, C. P.; Camp, P. J. Structure and Friction of Stearic Acid and Oleic Acid Films Adsorbed on Iron Oxide Surfaces in Squalane. *Langmuir* **2014**, *30* (1), 186−195.
(38) Shen, Y.-B.; Yu, K.-X.; Wang, Y.-J.; Qu, Y.-H.; Pan, L.-Q.; Cao, C.-F.; Cao, K.; Gao, J.-F.; Shi, Y.; Song, P.; Yong, J.; Hong, M.; Zhang, G.-D.; Zhao, L.; Tang, L.-C. Color adjustable, mechanically robust, flame-retardant and weather-resistant TiO2/MMT/CNF hierarchical nanocomposite coatings toward intelligent fire cyclic warning and protection. *Composites, Part B* **2024**, *271*, No. 111159.
(39) Nayak, S.; Chaki, T. K.; Khastgir, D. Dielectric relaxation and viscoelastic behavior of polyurethane-titania composites: dielectric mixing models to explain experimental results. *Polym. Bull.* **2017**, *74* (2), 369−392.
(40) Tao, P.; Viswanath, A.; Schadler, L. S.; Benicewicz, B. C.; Siegel, R. W. Preparation and Optical Properties of Indium Tin Oxide/Epoxy Nanocomposites with Polyglycidyl Methacrylate Grafted Nanoparticles. *ACS Appl. Mater. Interfaces* **2011**, *3* (9), 3638−3645.
(41) Ireni, N. G.; Karuppaiah, M.; Narayan, R.; Raju, K.; Basak, P. TiO2/Poly(thiourethane-urethane)-urea nanocomposites: Anticorrosion materials with NIR-reflectivity and high refractive index. *Polymer* **2017**, *119*, 142−151.

https://doi.org/10.1021/acsomega.4c01053
ACS Omega 2024, 9, 29339−29349